Journal of Magnetic Resonance 213 (2011) 176–181

Contents lists available at SciVerse ScienceDirect

Journal of Magnetic Resonance

journal homepage: www.elsevier.com/locate/jmr

Communication

Impact of gradient timing error on the tissue sodium concentration bioscale measured using flexible twisted projection imaging

Aiming Lu [a,*], Ian C. Atkinson [a], J. Thomas Vaughn [b], Keith R. Thulborn [a]

[a] Center for Magnetic Resonance Research, University of Illinois at Chicago, Chicago, IL 60612, United States
[b] Center for Magnetic Resonance Research, University of Minnesota, Minneapolis, MN 55455, United States

ARTICLE INFO

Article history:
Received 9 June 2011
Revised 12 August 2011
Available online 5 September 2011

Keywords:
Quantitative sodium imaging
Tissue sodium concentration
Gradient timing error
Flexible twisted projection imaging
Bioscale

ABSTRACT

The rapid biexponential transverse relaxation of the sodium MR signal from brain tissue requires efficient *k*-space sampling for quantitative imaging in a time that is acceptable for human subjects. The flexible twisted projection imaging (flexTPI) sequence has been shown to be suitable for quantitative sodium imaging with an ultra-short echo time to minimize signal loss. The fidelity of the *k*-space center location is affected by the readout gradient timing errors on the three physical axes, which is known to cause image distortion for projection-based acquisitions. This study investigated the impact of these timing errors on the voxel-wise accuracy of the tissue sodium concentration (TSC) bioscale measured with the flexTPI sequence. Our simulations show greater than 20% spatially varying quantification errors when the gradient timing errors are larger than 10 μs on all three axes. The quantification is more tolerant of gradient timing errors on the *Z*-axis. An existing method was used to measure the gradient timing errors with <1 μs error. The gradient timing error measurement is shown to be RF coil dependent, and timing error differences of up to ~16 μs have been observed between different RF coils used on the same scanner. The measured timing errors can be corrected prospectively or retrospectively to obtain accurate TSC values.

1. Introduction

Despite the number of MR sensitive nuclides that potentially report on brain metabolism, clinical MR neuroimaging remains focused on image contrast derived from water proton signals that are interpreted qualitatively, largely in terms of anatomy. Non-proton signals, such as from sodium that report on sodium ion homeostasis, can be quantified into metabolic parameters that have the potential to be interpreted quantitatively in terms of tissue viability under conditions of ischemia and during treatment of brain tumors [1–4]. Strategies for achieving quantitative sodium MR imaging to produce bioscales, defined as quantitative parametric maps interpretable directly in terms of biochemical processes, have been reported [5–10]. Despite the lower spatial resolution compared to proton MR images, such bioscales allow quantitative comparisons of metabolic processes between normal and diseased tissues across different patients and institutions [3–6]. The sources of errors in quantification must be identified and should be minimized.

Because of the short biexponential transverse relaxation (T2) properties of the sodium nucleus in tissue and the need to use long repetition times (ideally TR > 5T1) to avoid signal saturation for quantification purposes, imaging methods that allow for efficient spatial encoding with an ultra-short echo time (TE) must be used. These considerations led to the introduction of the 3D radial acquisition based twisted projection imaging (TPI) for quantitative sodium imaging [11]. TPI *k*-space trajectories are initially radial to move rapidly away from the oversampled center of *k*-space and then twist on the surface of a series of nested cones to acquire *k*-space samples uniformly distributed over the surface of spheres of increasing radii. TPI requires only a fraction of the total number of projections, or TR periods, that a corresponding critically sampled radial acquisition requires. Flexible TPI (flexTPI) extends TPI to achieve a flexible tradeoff between readout length and image resolution without violation of the gradient slew rate limits [9]. Other sequences such as 3D radial acquisition [12], 3D Cones [13,14], and density adapted radial acquisition [15] have also been proposed for sodium imaging. The 3D radial acquisition and density adapted radial acquisition require significantly more repetitions to critically sample *k*-space, limiting their applications for clinical quantitative 23Na imaging as the long TR values used to avoid signal saturation in this case would result in excessively long total acquisition times. In addition, both the 3D Cones sequence and TPI sequence sample *k*-space more evenly and are therefore have better signal-to-noise ratio (SNR) performance. The flexTPI sequence was used in this study due to its simpler gradient waveform design.

* Corresponding author. Address: Center for MR Research, 1801W, Taylor St., RM 1306 OCC (M/C 707), Chicago, IL 60612, United States. Fax: +1 312 355 3085.
E-mail address: aiminglu@uic.edu (A. Lu).

1090-7807/$ - see front matter © 2011 Elsevier Inc. All rights reserved.
doi:10.1016/j.jmr.2011.08.036

The impact of T1, T2, and B1 inhomogeneity on quantitative sodium imaging is well understood and can be properly addressed [5–9,16,17]. The importance of correcting for B0 inhomogeneity for sodium imaging has also been demonstrated recently [9]. However, although radial acquisition based imaging techniques are known to be sensitive to gradient timing errors and the effect of the gradient timing error on qualitative MR imaging of proton signals has been demonstrated [18–21], its impact on the accuracy of quantitative sodium imaging has not been reported. This is likely due to the fact that sodium imaging often uses relatively low acquisition bandwidth and has lower spatial resolution in order to achieve sufficient signal-to-noise ratio, therefore anatomical image distortions that arise from gradient timing errors are less apparent. However, as the TSC bioscale is proposed as a quantitative map, the sources of quantification error in this parameter must be defined. We report on the impact of the gradient timing error on the accuracy of quantification of tissue sodium concentration. Simulations using human brain sodium images show that quantification errors of greater than 20% can exist in TSC values without visible anatomical distortions when the gradient timing errors are greater than 10 μs on all three axes. Fortunately, this error is readily minimized by compensating for the timing errors with minimal scan time penalty.

2. Materials and methods

2.1. Gradient timing measurement

Unlike Cartesian-based imaging trajectories, radial acquisition based imaging techniques such as flexTPI, are sensitive to gradient timing errors that cause a delay in the onset of the *k*-space trajectories. This misalignment can result from multiple sources including non-zero phase responses of the analog and digital filters, gradient hardware delays, and eddy currents due to gradient switching [18]. The effect of the gradient timing error on qualitative MR imaging of proton and sodium signals has been demonstrated and correction strategies have been proposed [18–22]. Here, the gradient timing error was measured by relating it to the signal phases of the projections of the subject on each of the three physical axes, as proposed in the literature [18,21]. The pulse sequence diagram for the delay measurement is shown in Fig. 1a. The gradient timing error, t_d (shown in Fig. 1b), is related to the phases of the signals acquired with alternated gradient polarities in image space:

$$\arg(S^{+}(r)S^{-*}(-r)) = 2\gamma G t_d r + \phi \quad (1)$$

where $S^{+}(r)$ and $S^{-}(r)$ are the image space signals corresponding to the *k*-space signals acquired with positive and negative gradient polarities, respectively. G is the constant readout gradient amplitude, γ is gyromagnetic ratio of the nucleus being investigated, r is the spatial location of the spins along each of the three physical axes, and ϕ is a constant phase offset. The gradient timing error is found by linearly fitting Eq. (1) with respect to spatial location r scaled by $2\gamma G$.

As shown in Fig. 1c, these measured timing error values can be used to align the physical gradient waveforms and the timing of the analog–digital converter (ADC) readout. A negative measured t_d means the ADC starts after the physical gradient and therefore the logical gradient needs to be adjusted to start later relative to the ADC onset time in the pulse sequence. A positive t_d means the physical gradient starts after the ADC and therefore the logical gradient needs to be adjusted to start ealier relative to the ADC onset time. In either case, the necessary timing adjustment is $t_{adj} = -t_d$. The precision of this pre-compensation is 1 μs on our 3.0 T scanner (limited by hardware timing resolution of 2 μs).

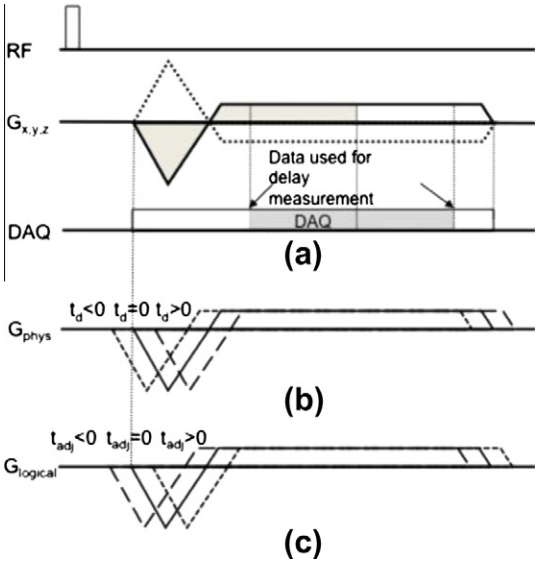

Fig. 1. (a) Timing diagram of the pulse sequence for the gradient delay measurement. The gradient waveform is only played out on one physical axis at a time. On each axis, two data acquisitions are performed with opposite gradient polarity (denoted by solid and dotted lines). The two shaded regions have equal areas. (b) Plots showing the physical gradient timing that could occur during data acquisition. While ideally the gradient should start at the same time as the ADC with delay time $t_d = 0$ (solid line) in this case, the physical gradient can also start before ($t_d < 0$, short dashed line) or after ($t_d > 0$, long dashed line) the start of the ADC. (c) Plots showing that the logical gradient can be moved before ($t_{adj} < 0$, long dashed line) or after ($t_{adj} > 0$, short dashed line) the onset time of the ADC in the pulse sequence to synchronize the physical gradient and the ADC.

Any residual timing errors can be incorporated into the image reconstruction, where retrospective timing correction is used to align the *k*-space data to the *k*-space trajectory. Preferably the prospective time correction performed at data collection ensures a small t_d so that the central *k*-space data are collected.

2.2. MR experiments

MR imaging was performed on a 3.0 T scanner (HDx, 14.0x, GE Healthcare, WI) equipped with broadband capabilities. The maximum gradient strength and slew rate of the system is 40 mT/m and 150 mT/m/s, respectively. Healthy adult subjects ($N = 5$, 4 male, aged 23–45 years) were recruited after obtaining informed consent for MR brain imaging. Unless otherwise mentioned, customized, identical single-tuned 23Na and 1H birdcage transmit/receive coils (16 rungs, inner diameter = 25.5 cm, length = 30.5 cm) were used in quadrature mode with capacitive coupling of the matching circuits to the coil. The subject's head was supported in an independent cantilevered head holder attached to the patient table. Thus these coils could be rapidly exchanged without subject motion to obtain co-registered datasets. For sodium experiments, the transmit power was manually adjusted to achieve a 90° flip angle with a 500 μs hard RF pulse. To examine the dependence of the timing measurement on the type of radiofrequency coil, the same experiments were also performed using a TEM sodium coil with an end-plate [23]. The inner diameter and the length of the cavity are 26.5 cm and 21.5 cm, respectively. The coil was operated in quadrature mode with capacitive coupling of the drive points to the coil.

2.2.1. Gradient timing measurement

To minimize the impact of B0 field inhomogeneities on gradient timing measurements, a spherical phantom filled with a sodium concentration of 56 mM was used. Shimming was performed using

the auto prescan procedure provided by the scanner manufacturer on the proton signal. The gradient timing measurements were performed along each of three axes at gradient amplitudes of 2, 4 and 8 mT/m. The gradient ramp time was kept constant (288 μs) in all experiments. The readout length was 8.192 ms (512 readout points with an acquisition bandwidth of 31.25 kHz. The dwell time was 16 μs with an oversampling factor of 2). The impact of short-term eddy currents on the delay measurement was minimized by using small encoding gradients and only the central 384 readout points for the measurement. The measured timing error values were then used to adjust the timing of the readout gradient waveforms during quantitative sodium imaging.

2.2.2. Quantitative sodium imaging

The imaging protocol is shown schematically in Fig. 2a. Proton imaging was always performed prior to sodium imaging to ensure that automated first order shimming was performed to optimize B0. This proton shimming was maintained for all subsequent proton and sodium imaging. A B0 map was then acquired for further correction of B0 inhomogeneities [24,25]. The B0 field map was obtained using 3D SPGR images with TE values of 2.1 ms and 4.3 ms in about one minute. This map was used to reconstruct sodium images after correction for the different gyromagnetic ratios of sodium and protons. The use of a B0 map based on protons rather than sodium shortened the time required for the human subject to remain stationary in the magnet. The RF coils were then exchanged and sodium imaging was performed with the flexTPI sequence with corrected gradient timing. A B1 map was obtained using the double flip angle method [26] to correct for B1 field inhomogeneity.

Imaging parameters for sodium imaging using the flexTPI sequence included TE = 0.36 ms (half of a constant 0.5 ms excitation RF pulse plus 0.11 ms hardware dead time after the RF pulse), FOV = 22 cm, bandwidth = 31.25 kHz, 5 mm isotropic nominal resolution, TR = 160 ms (full longitudinal relaxation for brain parenchyma where the measured T1 is ~30 ms [27]). The readout length was ~12.3 ms with a radial fraction of 0.25 and a maximum gradient strength of 0.4 G/cm. Two signal averages were used to improve the SNR. The total scan time for each sodium data acquisition was approximately 8 min for all *in vivo* studies. The total imaging time for a human subject was ~18 min which included shimming and two proton acquisitions (B1 map) and two sodium acquisitions (B1 map and quantifiable image) to obtain the final TSC bioscale.

The data acquisition was repeated with the same parameters on a sodium calibration phantom located at the same isocenter as the head and with a similar electrical loading of the RF coils as a human head. The calibration phantom consisted of a plastic sphere (4000 ml) containing three hollow cylindrical tubes (260 ml, inner diameter 5 cm) held in parallel along the main magnetic field within the center of the sphere. The cylinders were filled with different concentrations of sodium chloride (30, 70, 110 mM) in agar (3%) with the surrounding sphere filled with potassium chloride (60 mM). The methodology for quantifying the sodium signal is demonstrated in Fig. 2b and has been described previously [9]. This method using the calibration phantom minimizes errors in creating the calibration curve associated with B1 and B0 inhomogeneities.

2.3. Simulation of the effect of timing error on quantification

To demonstrate the impact of gradient timing error on quantification, the *k*-space trajectories for one dataset were recalculated by adjusting the readout gradient timing on all axes simultaneously in 4 μs intervals from −16 μs to 16 μs with respect to the start of data acquisition for both human and phantom sodium acquisitions in the dataset. This range was chosen based on the experimentally measured timing errors for the two sodium RF coils. The readout gradient on each individual axis was also shifted by different amount to examine the effect of anisotropic gradient delay on quantification. The corresponding *k*-space trajectories were then recalculated based on the shifted gradient waveforms and used to reconstruct both the calibration phantom and human sodium data. The resultant B1 and B0 corrected human images were then calibrated with the B0 and B1 corrected phantom images of known sodium concentrations to generate tissue sodium concentration bioscales.

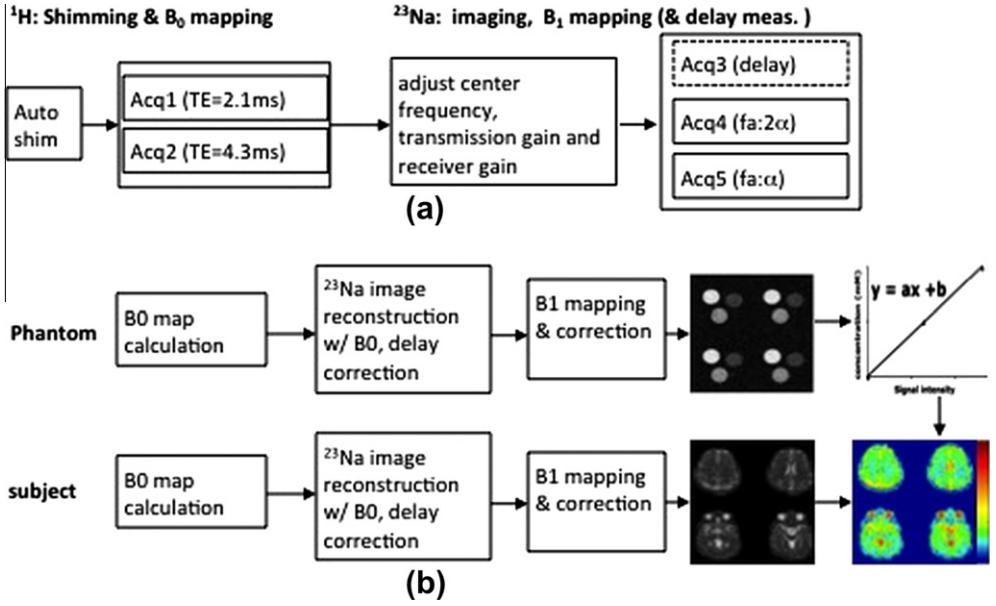

Fig. 2. (a) Illustration of the data acquisition steps and (b) flow chart of the image reconstruction and quantification processes for generating the tissue sodium concentration bioscale. The eddy current correction data can be collected beforehand on 1H data, assuming the 1H and the 23Na coils have the same eddy current characteristics.

3. Results

3.1. Timing error measurement

The measured timing delay errors for the sodium signal using the sodium birdcage coil and the sodium TEM coil at three different gradient strengths (2, 4 and 8 mT/m) on the *X*-, *Y*- and *Z*-axis are tabulated in Table 1. The averaged measured timing errors with the birdcage RF coil are: 0.0 ± 0.1, −1.7 ± 0.2 and 1.5 ± 0.1 μs on the *X*-, *Y*- and *Z*-axis, respectively, while those with the TEM coils are −8.7 ± 0.1, −11.4 ± 0.1, and −14.3 ± 0.2 μs, respectively. In both cases, the gradient timing errors are anisotropic on the three axes. The timing error values measured for the birdcage coil and the TEM coil are significantly different, likely due to different eddy current characteristics of the two coils. The birdcage coil is constructed using thin narrow stripes of copper to minimize eddy currents. The TEM coil is constructed with thick pieces of copper with a solid end-plate that support eddy currents.

3.2. Impact of gradient timing error on quantification

The impact of the isotropic timing errors along the three physical axes on tissue sodium quantification is shown in Fig. 3. Fig. 3a shows quantitative TSC maps generated with different delay times between gradient and the ADC when the same gradient delay was applied to all three axes. No significant anatomical distortion is seen in these images. The TSC values in the center of the FOV were underestimated when the ADC lagged the gradient waveform and overestimated when the ADC preceded the gradient waveform. The difference images in Fig. 3b clearly demonstrate lower TSC values for negative timing errors and higher TSC values for positive timing errors in the central brain region, while the opposite is observed at the edge of the brain.

The spatial dependence of TSC quantification error due to the timing mismatch for voxels on the horizontal line in the center of the images in Fig. 3a can be clearly appreciated in Fig. 4a, where the changes in TSC values for each voxel is plotted against the delay times. Each curve corresponds to one spatial location as indicated in Fig. 4b, a nearly linear relationship is observed in these plots. Substantial quantification error (up to ∼40%) is seen with a timing error of 16 μs along all three axes.

Fig. 5 demonstrates the impact on quantification of timing errors for each of the three physical axes separately. As expected, with the same timing error, the quantification errors are smaller when timing error is only present on one of the axis as compared to those in Fig. 3b. Quantification errors of up to 6 mmol/l tissue are seen in Fig. 5a and b with a timing error of 16 μs along either the *X*- or *Y*-axis, and the maximum quantification error in Fig. 5c is 3 mmol/l tissue with the 16 μs timing error along the *Z*-axis. The quantification errors are noticeably lower for a given timing error present on the *Z*-axis. The sensitivity of the accuracy of quantification to timing error on different axes is due to the flexTPI *k*-space acquisition strategy, where the axis of cones is parallel to *Z*-axis.

4. Discussion

The accuracy of quantifying the arbitrarily scaled magnitude sodium images into tissue sodium concentration bioscales depends on many factors such as the T1 and T2 of sodium in biological tissues, the accuracy of the sodium concentration in the calibration phantom, B0 inhomogeneity, B1 inhomogeneity, imaging SNR and the performance of the imaging hardware. Meaningful interpretation of quantitative sodium images requires proper accounting of these factors. The relatively short T1 values (∼30 ms) of the sodium signal from brain tissue permits signal saturation to be avoided by using TR values greater than 5T1. The short T2 requires use of short TE values with radial acquisition strategies to minimize signal loss. The impact of T2 signal loss on quantification is further reduced by closely matching the T2s of the calibration phantom to the average T2 values of brain parenchyma. The residual difference in T2 values between brain and the calibration phantom signals results in a systematic quantification bias that can be corrected with knowledge of the actual T2 values [28]. The uncertainty in the sodium concentrations of the gels is less than 1% with appropriate use of an accurate balance for solute weight measurements and volumetric flasks for solution preparation. The linearity of the calibration is verified by the high goodness of fit of the three-point calibration curve. No assumption of linearity has been made as would be required by a two-point calibration. The error from the calibration curve is thus determined by the SNR of phantom imaging which should be less than 1% as many (>100) voxels are averaged after B0 and B1 correction for each of the three calibration points. B0 inhomogeneity is often corrected by mapping the transmit field. Recently, B1 inhomogeneity correction has also been demonstrated to significantly improve quantitative sodium imaging with a flexTPI readout gradient [9]. Gradient timing errors are well known to introduce image blurring or distortion in qualitative proton imaging [17–20]. We have examined this error in our sodium imaging studies [9,21], but the impact of these gradient timing errors on the accuracy of quantification has not been previously reported. As shown in Fig. 3a, gradient timing errors do not introduce significant anatomical distortion or image quality degradation since quantitative sodium imaging is often performed with relatively low acquisition bandwidth and limited spatial resolution. However, when the misregistration of gradient time and ADC time is greater than 10 μs along all three axes, this error alone has been shown to result in a TSC error of more than 20% when using the 3D radial acquisition based pulse sequences when the calibration curve was derived from vials located in the middle of the FOV. Similar or even larger quantification errors are likely to occur when the calibration curve is to be obtained from vials

Table 1
Measured gradient timing errors on three physical axes with different gradient strengths using two RF coils. A negative measured t_d means the ADC starts before the physical gradient; while a positive t_d means the ADC starts after the physical gradient.

RF coil	Gradient strength (mT/m)	Measured timing error t_d (μs)		
		X	*Y*	*Z*
Birdcage coil	2	0.0	−1.6	1.5
	4	0.0	−1.7	1.4
	8	0.1	−1.9	1.5
	Mean	0.0 ± 0.1	−1.7 ± 0.2	1.5 ± 0.1
TEM coil	2	−8.8	−11.3	−14.4
	4	−8.7	−11.4	−14.1
	8	−8.7	−11.4	−14.4
	Mean	−8.7 ± 0.1	−11.4 ± 0.1	−14.3 ± 0.2

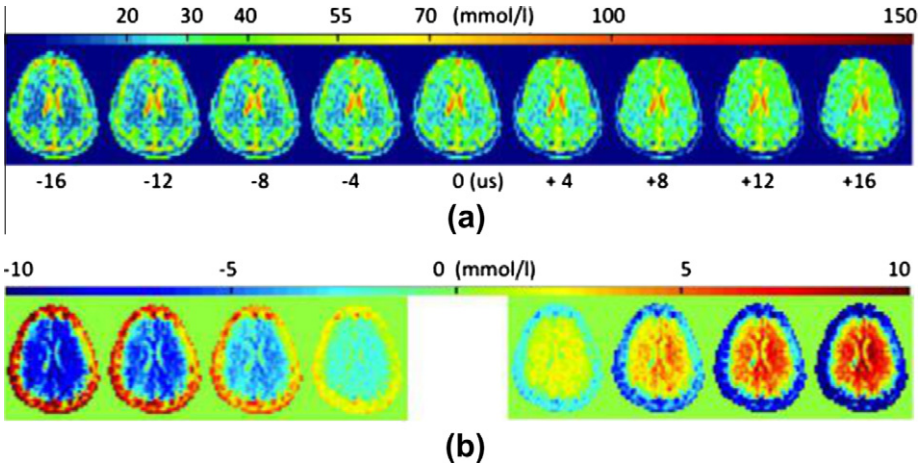

Fig. 3. (a) A representative section of sodium images of a human brain reconstructed with simulated delay times from −16 μs to 16 μs in 4 μs intervals from left to right on all three axes. The horizontal color scale is the tissue sodium concentration scale of 0–150 mmol/l tissue. (b) The corresponding difference images obtained by subtracting the original image from the images with different simulated delay times. The horizontal color scale is the difference in TSC in mmol/l tissue units.

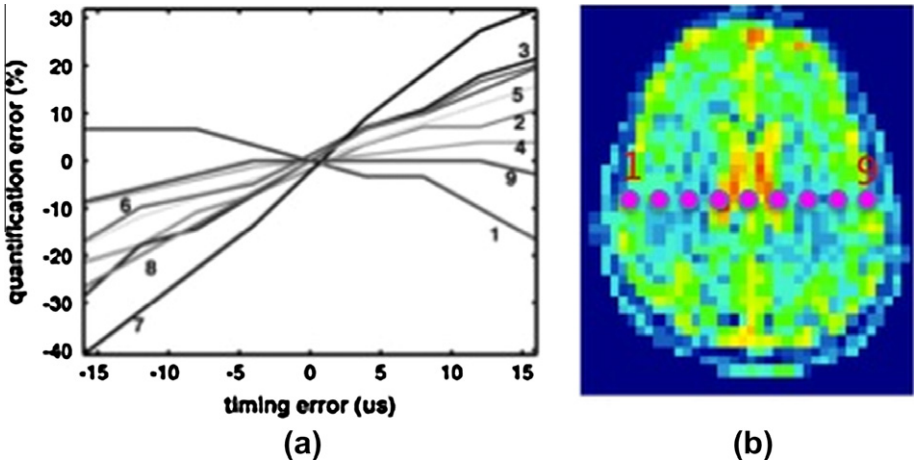

Fig. 4. (a) TSC quantification error (percent) due to timing error (μs) for voxels (1–9) lying along the horizontal central line through the representative TSC bioscale in (b). The locations of the voxels 1–9 are shown as magenta dots. The error is not uniform over the field of view.

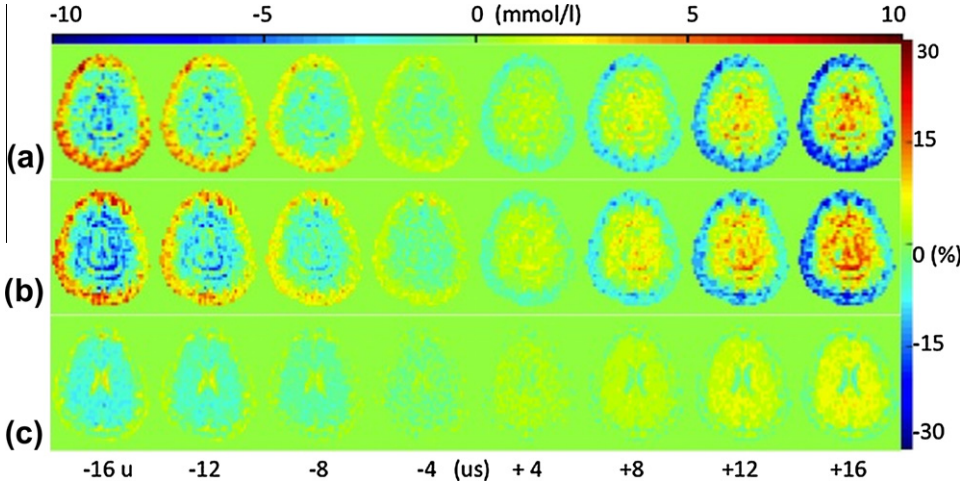

Fig. 5. (a) Quantification error for the same section of a human brain as Fig. 4 but with the delay timing errors of −16 μs to 16 μs in 4 μs intervals from left to right now played out along individual axes: (a) *X*-axis, (b) *Y*-axis and (c) *Z*-axis. The horizontal color scale is the TSC error with a range from –10 to +10 mmol/l tissue, while the vertical color scale is the percentage quantification error by normalizing the absolute error to a typical TSC value of 30 mmol/l.

located at the edge of the field of view [5], based on the signal intensity variation pattern across the field of view when gradient timing errors present. Therefore, pulse sequence timing must be carefully measured and adjusted to achieve accurate TSC measurement.

We have demonstrated that a simple, previously reported method can be used to measure the gradient delay with high precision. This method requires as few as 6 TR intervals to calculate the delay time for the three axes. The measured timing errors are relatively stable over time but are RF coil dependent. Each timing error can be measured with better than 1 μs precision as determined from repeated experiments and then corrected during data acquisition to within 1 μs based on the ADC timing resolution of our scanner. Residual timing errors after this correction can then be further compensated during imaging reconstruction by interpolating and shifting the *k*-space trajectories. This reduces the quantification error due to timing error to less than 1 mmol/l tissue in our simulations with a delay time of 1 μs. However, as the measured gradient timing errors are affected by eddy currents induced by the gradient in both the gradient coil and the RF coil, this method only corrects for the non-zero phase responses of the analog and digital filters, gradient hardware delays, and the average effect of eddy currents due to gradient switching. Eddy current correction by measuring the actual *k*-space trajectories is also needed if significant short-term or long-term eddy currents exist [9,22].

Although the results presented here were obtained using the flexTPI sequence, the same gradient timing error analysis and compensation strategies also apply to other radial acquisition based sequences such as 3D radial acquisition and 3D Cones.

5. Conclusion

The gradient timing error, if not corrected, can be a significant source of error in quantitative sodium imaging that will not be manifested in distortions of image geometry. At least in the setting of small eddy currents and small gradient strengths (i.e., twisted projection imaging), the correction parameter to minimize this error can be measured with minimal time penalty. The measured corrections can then be used both prospectively and retrospectively to align the collected data and the corresponding *k*-space trajectory to minimize this source of error in the TSC bioscale.

Acknowledgments

The authors gratefully acknowledge financial support from RO1 CA1295531A1 and a Spark award from the Chicago Biomedical Consortium and the Chicago Community Trust.

References

[1] K.R. Thulborn, J.J.H. Ackerman, Absolute molar concentrations by NMR in inhomogeneous B0: a scheme for analysis of in vivo metabolites, J. Magn. Reson. 55 (1983) 357–371.
[2] S.K. Hilal, A.A. Maudsley, J.B. Ra, H.E. Simon, P. Roschmann, S. Wittekoek, Z.H. Cho, S.K. Mun, In vivo NMR imaging of sodium-23 in the human head, J. Comput. Assist. Tomogr. 9 (1985) 1–7.
[3] K.R. Thulborn, D. Davis, J. Snyder, H. Yonas, A. Kassam, Sodium MR imaging of acute and subacute stroke for assessment of tissue viability, Neuroimag. Clin. N. Am. 15 (2005) 639–653.
[4] K.R. Thulborn, Aiming Lu, I.C. Atkinson, F. Damen, J.L. Villano, Quantitative sodium MR imaging and sodium bioscales for the management of brain tumors, Neuroimag. Clin. N. Am. 19 (4) (2009) 615–624.
[5] R. Ouwerkerk, K.B. Bleich, J.S. Gillen, M.G. Pomper, P.A. Bottomley, Tissue Sodium concentration in human brain tumors as measured with 23Na MR imaging, Radiology 227 (2003) 529–537.
[6] C.D. Constantinides, D.L. Kraitchman, K.O. O'Brien, F.E. Boada, J. Gillen, P.A. Bottomley, Noninvasive quantification of total sodium concentrations in acute reperfused myocardial infarction using 23Na MRI, Magn. Reson. Med. 46 (2001) 1144–1151.
[7] F.E. Boada, J.S. Gillen, D.C. Noll, G.X. Shen, K.R. Thulborn, Data acquisition and postprocessing strategies for fast quantitative sodium imaging, Int. J. Imag. Syst. Technol. 8 (1997) 544–550.
[8] R. Ouwerkerk, R.G. Weiss, P.A. Bottomley, Measuring human cardiac tissue sodium concentrations using surface coils, adiabatic excitation, and twisted projetion imaging with minimal T2 losses, J. Magn. Reson. Imag. 21 (2005) 546–555.
[9] A. Lu, I.C. Atkinson, T. Claiborne, F.C. Damen, K.R. Thulborn, Quantitative sodium imaging with a flexible twisted projection pulse sequence, Magn. Reson. Med. 63 (2010) 1583–1593.
[10] K.R. Thulborn, T.S. Gindin, D. Davis, P. Erb, Comprehensive MRI protocol for stroke management: tissue sodium concentration as a measure of tissue viability in a non-human primate model and clinical studies, Radiology 139 (1999) 26–34.
[11] F. Boada, J. Gillen, G. Shen, S. Chang, K. Thulborn, Fast three dimensional sodium imaging, Magn. Reson. Med. 37 (1997) 706–715.
[12] R. Jerecic, M. Bock, S. Nielles-Vallespin, C. Wacker, W. Bauer, L.R. Schad, ECG-gated 23Na-MRI of the human heart using a 3D-radial projection technique with ultra-short echo times, MAGMA 16 (2004) 297–302.
[13] P.T. Gurney, B.A. Hargreaves, D.G. Nishimura, Design and analysis of a practical 3D cones trajectory, Magn. Reson. Med. 55 (March) (2006) 575–582.
[14] E. Staroswiecki, N.K. Bangerter, P.T. Gurney, T. Grafendorfer, G.E. Gold, B.A. Hargreaves, In vivo sodium imaging of human patellar cartilage with a 3D cones sequence at 3 T and 7 T, J. Magn. Reson. Imag. 32 (2010) 446–451.
[15] A.M. Nagel, F.B. Laun, M.A. Weber, C. Matthies, W. Semmler, L.R. Schad, Sodium MRI using a density-adapted 3D radial acquisition technique, Magn. Reson. Med. 62 (2009) 1565–1573.
[16] G. Steidle, H. Graf, F. Schick, Sodium 3D-MRI of the human torso using a volume coil, Magn. Reson. Imag. 22 (2004) 171–180.
[17] L. Wang, Y. Wu, G. Chang, N. Oesingmann, M.E. Schweitzer, A. Jerschow, R.R. Regatte, Rapid isotropic 3D-sodium MRI of the knee joint in vivo at 7 T, J. Magn. Recon. Imag. 30 (2009) 606–614.
[18] S.B. Reeder, A.Z. Faranesh, E. Atalar, E.R. McVeigh, A novel object-independent balanced reference scan for echo-planar imaging, J. Magn. Reson. Imag. 9 (6) (1999) 847–852 (June).
[19] C.B. Ahn, Zh Cho, A new phase correction method in NMR imaging based on autocorrelation and histogram analysis, IEEE Trans. Med. Imag. 6 (1987) 32–36.
[20] D.C. Peters, J.A. Derbyshire, E.R. McVeigh, Centering the projection reconstruction trajectory: reducing gradient delay errors, Magn. Reson. Med. 50 (2003) 1–6.
[21] O. Wieben, E. Brodsky, C.A. Mistretta, W.F. Block, Correction of trajectory errors in radial acquisitions, in: Proceedings of International Society of Magnetic Resonance Medicine, Toronto, 2003, p. 298.
[22] I.C. Atkinson, A. Lu, K.R. Thulborn, Characterization and correction of system delays and eddy currents for MR imaging with ultrashort echo-time and time-varying gradients, Magn. Reson. Med. 62 (2009) 532–537.
[23] J.T. Vaughan, G. Adriany, M. Garwood, E. Yacoub, T. Duong, L. DelaBarre, P. Andersen, K. Ugurbil, Detunable transverse electromagnetic (TEM) volume coil for high-field NMR, Magn. Reson. Med. 47 (2002) 990–1000.
[24] D.C. Noll, C.H. Meyer, J.M. Pauly, D.G. Nishimura, A. Macovski, Deblurring for non-2D Fourier transform magnetic resonance imaging, Magn. Reson. Med. 25 (1992) 319–333.
[25] L.C. Man, J.M. Pauly, A. Macovski, Multifrequency interpolation for fast off-resonance correction, Magn. Reson. Med. 37 (1997) 785–792.
[26] E.K. Insko, L. Bolinger, Mapping of the radiofrequency field, J. Magn. Recon. 103 (1993) 82–85.
[27] R. Ouwerkerk, R.H. Morgan, 23Na MRI: from research to clinical use, J. Am. Coll. Radiol. 4 (2007) 739–741.
[28] I.C. Atkinson, A. Lu, K.R. Thulborn, Clinically constrained optimization of flexTPI acquisition parameters for the tissue sodium concentration bioscale, Magn. Reson. Med. (2011), doi:10.1002/mrm.22908.